PHOTONICS Research

High-speed and high-power germanium photodetector with a lateral silicon nitride waveguide

Xiao Hu,[1,2] Dingyi Wu,[2] Hongguang Zhang,[1] Weizhong Li,[1,2] Daigao Chen,[1,2] Lei Wang,[1,2] Xi Xiao,[1,2,*] and Shaohua Yu[1,2]

[1]National Information Optoelectronics Innovation Center, China Information and Communication Technologies Group Corporation (CICT), Wuhan 430074, China
[2]State Key Laboratory of Optical Communication Technologies and Networks, China Information and Communication Technologies Group Corporation (CICT), Wuhan 430074, China
*Corresponding author: xxiao@wri.com.cn

Received 15 December 2020; revised 19 February 2021; accepted 1 March 2021; posted 1 March 2021 (Doc. ID 417601); published 26 April 2021

Up to now, the light coupling schemes of germanium-on-silicon photodetectors (Ge-on-Si PDs) could be divided into three main categories: (1) vertical (or normal-incidence) illumination, which can be from the top or back of the wafer/chip, and waveguide-integrated coupling including (2) butt coupling and (3) evanescent coupling. In evanescent coupling the input waveguide can be positioned on top, at the bottom, or lateral to the absorber. Here, to the best of our knowledge, we propose the first concept of Ge-on-Si PD with double lateral silicon nitride (Si_3N_4) waveguides, which can serve as a novel waveguide-integrated coupling configuration: double lateral coupling. The Ge-on-Si PD with double lateral Si_3N_4 waveguides features uniform optical field distribution in the Ge region, which is very beneficial to improving the operation speed for high input power. The proposed Ge-on-Si PD is comprehensively characterized by static and dynamic measurements. The typical internal responsivity is evaluated to be 0.52 A/W at an input power of 25 mW. The equivalent circuit model and theoretical 3 dB opto-electrical (OE) bandwidth investigation of Ge-on-Si PD with lateral coupling are implemented. Based on the small-signal (S21) radio-frequency measurements, under 4 mA photocurrent, a 60 GHz bandwidth operating at −3 V bias voltage is demonstrated. When the photocurrent is up to 12 mA, the 3 dB OE bandwidth still has 36 GHz. With 1 mA photocurrent, the 70, 80, 90, and 100 Gbit/s non-return-to-zero (NRZ) and 100, 120, 140, and 150 Gbit/s four-level pulse amplitude modulation clear openings of eye diagrams are experimentally obtained without utilizing any offline digital signal processing at the receiver side. In order to verify the high-power handling performance in high-speed data transmission, we investigate the eye diagram variations with the increase of photocurrents. The clear open electrical eye diagrams of 60 Gbit/s NRZ under 20 mA photocurrent are also obtained. Overall, the proposed lateral Si_3N_4 waveguide structure is flexibly extendable to a light coupling configuration of PDs, which makes it very attractive for developing high-performance silicon photonic integrated circuits in the future.

https://doi.org/10.1364/PRJ.417601

1. INTRODUCTION

Silicon photonics is a fascinating technology to realize large-scale electronics-photonics integration on a chip with low cost, high bandwidth, large volume, high energy efficiency, and complementary metal-oxide semiconductor (CMOS) compatibility [1–5]. Silicon photonics has been proving its great worth in data centers, long-haul telecommunication, integrated quantum communication, integrated microwave photonics, artificial intelligence (AI), and high-performance computers [2,4–8].

One of the key building blocks of silicon photonics is photodetectors (PDs) that convert high-speed optical signals to electrical signals [9,10]. However, the intrinsic properties of silicon (Si), an indirect band-gap semiconductor with a band-gap energy of 1.1 eV which is transparent in the near-IR wavelength band (1.3–1.55 μm), make it challenging to realize photodetection [10]. As an option, germanium (Ge), which possesses great linear absorption up to 1550 nm and can be extended up to 2000 nm by exploiting tensile-strained germanium-on-silicon (Ge-on-Si) bandgap shrinkage, has appeared as a prime

choice for photodetection [11–14]. The measured absorption coefficients of Ge material are about 10^4 cm^{-1} at 1310 nm and 5×10^3 cm^{-1} at 1550 nm [15,16]. The chief drawback of the 4.2% lattice mismatch between Ge and Si, which will result in a high misfit dislocation density and make it difficult to achieve the high-quality epitaxial growth of thick Ge on Si, has been alleviated by employing the technique of two-step Ge epitaxial deposition and continuous or cyclic thermal treatment [10,11,13,17–19]. In recent years, with different approaches developed to realize high-quality epitaxial growth Ge on Si, a variety of Ge-on-Si PDs have been designed and demonstrated, mainly focusing on p-i-n (PIN) [20] and metal-semiconductor-metal (MSM) devices [21].

Generally speaking, there are existing three types of light illuminating Ge-on-Si PDs [16,22,23]: (1) vertical (or normal-incidence) illumination for fiber-optic coupling or free space [22,24], which can be from the top or back of the wafer/chip, and waveguide-integrated coupling including (2) butt coupling and (3) evanescent coupling as shown in Fig. 1. In evanescent coupling the input optical waveguide can be positioned on top, at the bottom, or lateral to the absorber. Various high-speed waveguide-integrated Ge-on-Si PDs have been comprehensively investigated [14,25–29]. For the butt-coupling scheme, the Ge absorption region also serves as an extended part of the optical waveguide [28–30]. A lateral heterostructured Si-Ge-Si junction PD operating at 25 Gbit/s has been experimentally reported [28]. For the evanescent-coupling scheme with the input waveguide positioned at the bottom to the absorber, the light is evanescently coupled to Ge absorption region [13,14,26,27,31,32]. The 100 Gbit/s on-off-keying (OOK) data reception detector with evanescent coupling (bottom) is demonstrated by IMEC [14]. However, the Si-contacted Ge waveguide PD needs to etch the 220 nm Si and grow poly-Si taper, which may increase fabrication difficulty and cost. Also, the nonuniform optical field distribution in the Ge absorption region may be harmful to carrier transport, especially for high optical input power. For the evanescent-coupling scheme with the input waveguide positioned on top of the absorber, the light can also be evanescently coupled to the Ge absorption region with the condition of phase matching [23,33]. It possesses the ability to independently manipulate the light field. Nevertheless, the experimentally demonstrated silicon nitride (Si_3N_4) waveguide-based PD only has a 3 dB bandwidth of 7.2 GHz at 1 V reverse bias voltage [23]. The evanescent-coupling scheme with the Si waveguide positioned lateral to the absorber [34] features high-power and high-speed photodetection with mode-evolution-based structure. At a total input power of 4 mW, the opto-electrical (OE) bandwidth of 31 GHz is experimentally demonstrated.

Compared to a Si waveguide, the Si_3N_4 waveguide features a large band gap and absence of two-photon or free-carrier absorption in the telecom band, ultralow propagation loss (<1 dB/m), as well as low nonlinearity and a wide-band transparency window (0.4–4.5 μm) [35–38]. Additionally, several major foundries, such as AIM Photonics, CompoundTek, ST Microelectronics, and CEA-Leti, have pronounced their silicon photonic platforms integrated with at least one Si_3N_4 layer. However, the combining of Ge-on-Si PD with Si_3N_4 waveguides has not been explored much. Especially, to the best of the authors' knowledge, a Ge-on-Si PD with a double lateral coupling scheme has not been proposed and demonstrated.

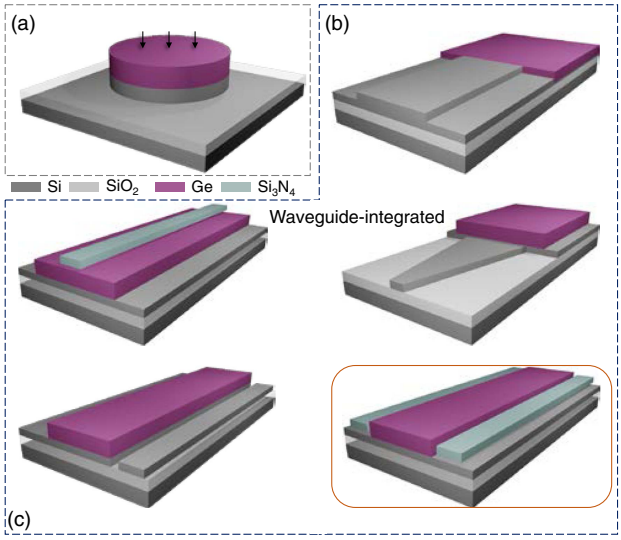

Fig. 1. Three optical coupling schemes of Ge-on-Si PD: (a) vertical incidence and waveguide-integrated coupling including (b) butt coupling and (c) evanescent coupling. In evanescent coupling the optical input waveguide can be positioned on top, at the bottom, or lateral to the absorber (germanium). The inside of the orange rectangle is the evanescent-coupling configuration based on double lateral Si_3N_4 waveguides, which is first proposed and demonstrated in this work.

In this paper, we report the first concept of a Ge-on-Si PD with double lateral Si_3N_4 waveguides, which can serve as a novel waveguide-integrated coupling configuration as shown in Fig. 1. The double lateral coupling Si_3N_4 waveguides will decouple the light propagation from the Ge absorption and Si slab waveguide. They allow for independent optimization of quantum efficiency, operation speed, and power handling. The Ge-on-Si PD based on lateral coupling Si_3N_4 waveguides has several distinctive advantages. (1) The lateral Si_3N_4 waveguides can be designed relatively free. This might be very beneficial to manipulating the optical field in the Ge absorption region to attain uniform photocarrier distribution, which will be helpful to improve quantum efficiency and operation speed. (2) The light propagation in the double lateral Si_3N_4 waveguides will avoid the optical loss caused by bottom doped silicon slab waveguide. The doping density of the silicon slab waveguide can be appropriately adjusted to achieve higher operation speed again. (3) As the $\chi^{(3)}$ of Si_3N_4 is about 20 times lower than that of Si in the telecommunication wavelength range, the light propagation in the double lateral Si_3N_4 waveguides possesses lower nonlinearity [35]. Therefore, the Si_3N_4 waveguide can sustain higher optical power density than the Si waveguide and evade two-photon absorption, which means wide-input-power dynamic range. (4) The combination of high-speed Ge-on-Si PD with a Si_3N_4 waveguide could be a novel active Si_3N_4 platform that could achieve the integration of coherent receivers at 1 μm and the visible light band.

We design and fabricate the Ge-on-Si PD with double lateral coupling Si_3N_4 waveguides based on a commercial standard silicon-on-insulator (SOI) platform. To comprehensively characterize the proposed lateral coupling Ge-on-Si PD, first, the static current-voltage (*I-V*) characteristic and responsivity are measured. Then equivalent circuit model and theoretical 3 dB OE bandwidth investigation are implemented. Second, the small-signal (S21, S11) radio-frequency (RF) measurements for the Si_3N_4-based lateral coupling PD are executed. Finally, the high-speed and high-power large-signal measurements, including non-return-to-zero (NRZ) on-off-keying (OOK) and four-level pulse amplitude modulation (PAM-4) eye diagrams are attained.

2. STRUCTURE AND PRINCIPLE

Figure 1 shows the reported three waveguide-integrated light coupling schemes of Ge-on-Si PDs: (a) vertical (or normal-incidence) illumination and waveguide-integrated coupling including (b) butt coupling and (c) evanescent coupling. Based on the phase matching of a leaky-mode model, which could be used to study evanescent wave coupling behavior between low-index Si_3N_4 and high-index Ge [33], the Ge-on-Si PD with double lateral Si_3N_4 waveguides is proposed and designed. In this work, we propose a concept of realizing the novel light coupling configuration: lateral coupling by using double lateral Si_3N_4 waveguides as shown in Fig. 1(c). Figure 2(a) depicts the more detailed three-dimensional (3D) schematic of the Ge-on-Si PD with double lateral Si_3N_4 waveguides. Figure 2(b) shows the top view of the proposed PD structure; the width and length of the Ge active region are 2.5 μm and 20 μm, respectively. The light is injected into the lateral Si_3N_4 waveguides and can then be evanescently coupled to Ge region. The gap between the lateral Si_3N_4 waveguide and the Ge region is estimated to be 150 nm. The thickness of the Si_3N_4 layer is 400 nm, and the Si_3N_4 waveguide is linearly tapered from 800 to 450 nm. Figure 2(c) shows a cross-sectional view of the Ge-on-Si PD with lateral Si_3N_4 waveguides. The gap from the bottom edge of the Si_3N_4 waveguide to the top edge of Si is about 400 nm, which is determined by foundry fabrication processes. The Ge-on-Si PD is fabricated on a commercial standard SOI platform, with 0.22 μm Si and 8 μm buried oxide (BOX) layers. A 450 nm height Ge film is grown on the 220 nm Si layer, with its top 150 nm ion implanted by N+ for ohmic contact. The bottom 220 nm thick Si waveguide is implanted by P and P+ for ohmic contact. The doping concentrations of the N+ and P regions are estimated to be 4×10^{18} cm^{-3} and 2×10^{18} cm^{-3} to improve operation speed. The pair of positive and negative electrodes can provide a strong electrostatic field in the Ge region, ensuring efficient and fast collection of photogenerated carriers.

For regular butt-coupling and evanescent-coupling (bottom) schemes, the light is injected into Ge region all at once with nonuniform optical field distribution in the absorber, which will cause a large electron–hole pair density at the Ge-Si waveguide interface [13,25]. The high density of photogenerated electron–hole pairs generates relatively strong gradient of charge, which will induce a large electric field opposing to the applied external voltage. This phenomenon is called carrier screening [39,40], which will drastically degrade the 3 dB OE bandwidth. Therefore, the uniform optical field distribution in the Ge region will be helpful to generate homogeneous electron–hole pair density, and consequently, it is beneficial to improving the operation speed. Figure 2(d) shows the cross-sectional view of field distribution of the Si_3N_4 waveguide with 800 nm and 450 nm width and the side view of field distribution of the Ge absorption region. The light propagates along the *x* axis. Compared with butt coupling and evanescent coupling (bottom), it is obvious that the light spreads more uniformly in the whole Ge absorption region by using double lateral Si_3N_4 waveguides.

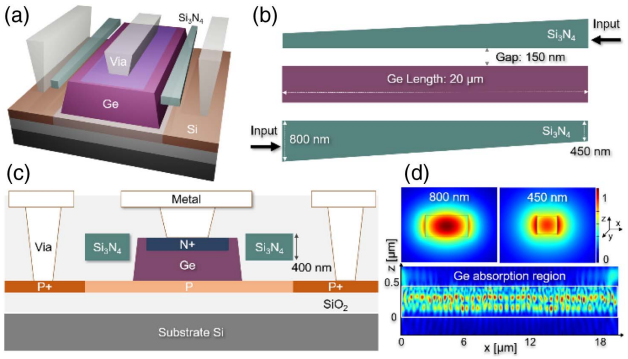

Fig. 2. (a) Three-dimensional (3D) schematic of Ge-on-Si PD with double lateral Si_3N_4 waveguides. (b) Top view of Ge-on-Si PD with double lateral Si_3N_4 waveguides. (c) Cross-sectional view of Ge-on-Si PD with double lateral Si_3N_4 waveguides. (d) Cross-sectional view of the Si_3N_4 waveguide optical field with 800 nm and 450 nm width and the side view of the optical field distribution of the Ge absorption region. The light propagates along the *x* axis.

3. EXPERIMENTAL RESULTS

A. Optical Micrograph and Setups

Figure 3(a) shows the optical micrograph of the fabricated Ge-on-Si PD with double lateral Si_3N_4 waveguides. The input light was first coupled from a single-mode fiber through the grating coupler, and then split by a silicon-based 1×2 multi-mode interferometer (MMI). The Si to Si_3N_4 inter-layer transitions, which are designed as adiabatic mode transformers around 1550 nm, are used to efficiently couple light from the Si waveguide to the Si_3N_4 waveguide. Finally, the light can be uniformly coupled to the Ge absorption region through double lateral Si_3N_4 waveguides. Schematics of the experimental setups for the measurement of the 3 dB OE bandwidth and eye diagrams are illustrated in Figs. 3(b) and 3(c). The 3 dB OE bandwidth of the Ge-on-Si PD with double lateral Si_3N_4 waveguides is evaluated from the S-parameter (S21) using a 67 GHz lightwave component analyzer (LCA, Keysight N4373D). The arbitrary waveform generator (AWG) generates pseudorandom binary sequence (PRBS) of order 15 and is then amplified by a 67 GHz driver. The continuous optical wave with 10 dBm power at 1.55 μm is generated by a commercial Keysight laser and is then injected into one polarization controller (PC1). The 6 dB bandwidth of the 40 GHz lithium niobite ($LiNbO_3$) Mach–Zehnder modulator operating at 1.55 μm is driven

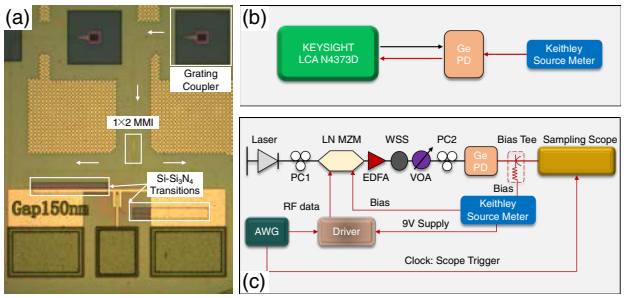

Fig. 3. (a) Micrograph of the fabricated Ge-on-Si PD with double lateral Si_3N_4 waveguides. (b) and (c) Schematic of the experimental setup for the measurement of the 3 dB OE bandwidth and eye diagrams. The black and red lines represent the optical and electrical connections, respectively. PD, photodetector; AWG, arbitrary waveform generator; EDFA, erbium-doped fiber amplifier; VOA, variable optical attenuator; WSS, wavelength-selective switch; PC, polarization controller; LN MZM, lithium niobite Mach–Zehnder modulator.

by the amplified RF data. The modulated high-speed optical signal is amplified, filtered, and injected into the low-loss variable optical attenuator (VOA). Since the input grating coupler is polarization sensitive, the modulated high-speed optical signal is then injected into the other PC2, and the designed Ge-on-Si PD with lateral Si_3N_4 waveguides converts it to photocurrent. The sampling scope with 50 Ω termination converts the photocurrent into the voltage. The Ge-on-Si PD with double lateral Si_3N_4 waveguides is direct current (DC) biased by a 67 GHz bias tee.

B. Static Measurements

A typical static current-voltage (*I-V*) characteristic of the proposed Ge-on-Si PD in the dark illuminated state is shown in Fig. 4(a). The device exhibits dark current as low as 7 nA and 84 nA at −1 V and −3 V. To evaluate the optical absorption capability of Ge-on-Si PD, the photocurrent was measured as a function of the input optical power at 1550 nm with −1 V bias voltage as depicted in the Fig. 4(b). Here, the losses of the grating coupler, silicon single-mode waveguides, 1 × 2 MMI splitter, and Si to Si_3N_4 inter-layer transition are about 6 dB/port, 2 dB/cm, 0.3 dB, and 0.2 dB, respectively. The internal responsivity is evaluated to be approximately 0.4 A/W at 1550 nm with 2 mW input power, showing a relatively low quantum efficiency $\eta = 32\%$, defined as follows: $\eta = (R \times 1.24)/\lambda$, where R and λ are the responsivity and operating wavelength. The relatively low quantum efficiency is mainly attributed to the optical absorption losses caused by metal copper and low-efficiency coupling. As shown in Fig. 2(c), the gap between the metal copper and the Si_3N_4 waveguide is about 300 nm, which is determined by the process flow of the commercial standard SOI waveguide platform. Therefore, the metal copper will cause the loss of the Si_3N_4 optical waveguide. Additionally, in the vertical direction, the gap from the bottom edge of the Si_3N_4 waveguide to the top edge of Si is 400 nm, which means that the overlap between the Ge absorption region and the Si_3N_4 waveguide is less than 100 nm. The small overlap region may also lead to low-efficiency coupling. We believe that the decreasing of the gap between the Si_3N_4 waveguide and the Si and the increasing of the gap between the Si_3N_4 waveguide

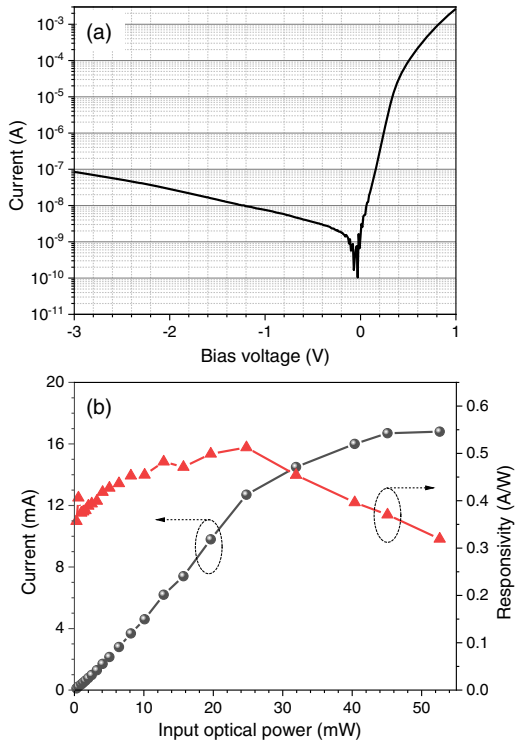

Fig. 4. (a) Current-voltage (*I-V*) characteristics of Ge-on-Si PD with double lateral Si_3N_4 waveguides in the dark illuminated state. (b) Measured photocurrent and responsivity as a function of input optical power at −1 V bias voltage.

and the metal copper will significantly improve the quantum efficiency of the proposed Ge-on-Si PD. As shown in Fig. 4(b), there was a good linear relationship between photocurrent versus optical power before the input power up to 25 mW. The maximum responsivity is estimated to be 0.52 A/W. Past 25 mW of input power, the saturated absorption effect in the photocurrent was obviously observed. When the input power is 52 mW, the Ge-on-Si PD with double lateral Si_3N_4 waveguides produces 17 mA of photocurrent and realizes the increase of the saturation current by more uniformly illuminating the Ge absorption.

C. Equivalent Circuit Model

The extracted equivalent circuit model can explain the influence of various parameters on PD performances. Furthermore, such a model is very useful for optimal design of simultaneous high speed and high sensitivity. The inset in Fig. 5(a) plots the extracted equivalent circuit model of our proposed Ge-on-Si PD with lateral Si_3N_4 waveguides, where C_j is the total junction capacitance, C_p is the parasitic capacitance, and R_s is the series resistance. In order to extract C_j, C_p, and R_s, the S11 parameters are measured from 100 MHz to 60 GHz using an LCA under −3 V bias voltage. Figure 5 shows the experimental and fitted magnitude/phase part of the small-signal S11 reflection parameters. The series resistance and total capacitance of a Ge-on-Si PD with lateral Si_3N_4 waveguides are extracted by fitting the S11 scattering parameter data to the small-signal RC-model. The fitting result exhibits good

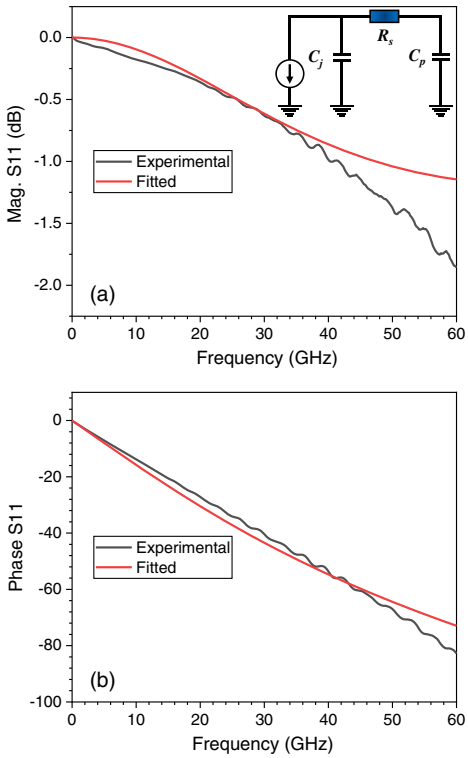

Fig. 5. (a) and (b) Experimental and fitted magnitude/phase part of the small-signal S11 reflection parameters from 100 MHz to 60 GHz at −3 V bias voltage. The inset plots the extracted equivalent circuit model of our proposed Ge-on-Si PD with lateral Si_3N_4 waveguides.

agreement with the measured scattering parameter data curve, which results in a junction capacitance C_j of 17.6 fF, series resistance R_s of 20 Ω, and parasitic capacitance C_p of 10 fF at −3 V bias voltage. The load resistance R_{load} is 50 Ω.

D. Theoretical 3 dB OE Bandwidth

To profoundly analyze the high-frequency response of the fabricated Ge-on-Si PD with double lateral Si_3N_4 waveguides, first, the theoretical calculation of the 3 dB OE bandwidth is presented. Then the small-signal measurements for the Ge-on-Si PD are implemented. It is well known that the RF response of a Ge-on-Si PD is largely controlled by carrier transit-time-limited bandwidth (f_{tr}) and resistor-capacitor (RC)-limited bandwidth (f_{RC}) in the active PIN regions [27,41]. The carrier transit frequency f_{tr} can be written as

$$f_{\text{tr}} = \frac{0.45 v_b}{d}, \tag{1}$$

where v_b is the carrier saturation drift velocity (Ge: $v_b = 6 \times 10^6$ cm/s) and d is the thickness of the intrinsic Ge zone. For the proposed Ge-on-Si PD with double lateral Si_3N_4 waveguides, the intrinsic Ge (i-Ge) region is about 0.3 μm. Therefore, the theoretical f_{tr} is estimated to be 90 GHz. The limit of the RC bandwidth can be calculated by [27,41]

$$f_{\text{RC}} = \frac{1}{2\pi RC}, \tag{2}$$

where R is the total resistance, which includes the series resistance R_s and the load resistance R_{load}, and C is the capacitance, including the junction capacitance C_j and the parasitic capacitance C_p. Based on the extracted parameters (R and C) from the S11 measurement, the f_{RC} is evaluated to be approximately 82.4 GHz.

The total 3 dB frequency response, determined by f_{tr} and f_{RC}, can be calculated by [41,42]

$$f_{3\,\text{dB}} = \frac{1}{\sqrt{f_{\text{RC}}^{-2} + f_{\text{tr}}^{-2}}}. \tag{3}$$

Therefore, the theoretical 3 dB OE bandwidth $f_{3\,\text{dB}}$ of a Ge-on-Si PD with lateral Si_3N_4 waveguides is evaluated to be approximately 60.8 GHz.

E. Small-Signal Measurements

In order to experimentally verify the 3 dB OE bandwidth of Ge-on-Si PD coupling with double lateral Si_3N_4 waveguides, we implemented small-signal RF measurements. The calibration of the high-speed RF trail was implemented to consider the contributions from GSG probes and coaxial cables. The small-signal measurement setup is depicted in Fig. 3(b). The bandwidth test experiments were achieved by collecting the response of the S21 transmission parameter in the LCA tool versus frequency with different photocurrents under 3 V reverse-bias voltage as depicted in Fig. 6(a). Figure 6(b) shows the measured 3 dB OE bandwidths with different photocurrent levels. By fitting the experimental result of the S21 transmission parameter under 4 mA photocurrent, as shown in the inset of Fig. 6(b), the maximum 3 dB bandwidth of 60 GHz is realized, which is well matched to the theoretically estimated 60.8 GHz. The black curve represents the experimental result of the S21 transmission parameter. Based on the polynomial fit function, which is provided by commercial software, the red curve of the Fig. 6(b) inset was obtained. The 3 dB OE bandwidths slowly increase with the photocurrent from 1 to 4 mA. With the photocurrents further increasing, the bandwidths gradually reduce. When the photocurrent up to 12 mA, the 3 dB OE bandwidth of Ge-on-Si PD with double lateral Si_3N_4 waveguides still has 36 GHz. This is benefitting from the uniform optical field distribution in the Ge region as shown in Fig. 2(d). The photogenerated carriers can be swept out of the absorption zone effectively. Then the carrier transit time increases not very significantly. The experimentally demonstrated ultrahigh 3 dB OE bandwidth under large photocurrent sufficiently proves the validity of the double lateral optical coupling technique for high-speed and high-power data reception.

F. Large-Signal Eye Diagram Measurements

The feasibility of this Ge-on-Si PD with double lateral Si_3N_4 waveguides was further checked by measuring the eye-diagram large-signal acquisitions with different operation speed and input optical power. The data were transmitted in NRZ and PAM-4 optical modulation formats. A (2^{15} − 1) long optical NRZ PRBS data pattern at 70, 80, 90, and 100 Gbit/s, generated by a commercial $LiNbO_3$ modulator at 1550 nm, was amplified by using a C-band erbium-doped fiber amplifier (EDFA) and followed by a filter (wavelength-selective switch, WSS) to reduce spontaneous emission noise. The bandwidth and insertion loss of the em-

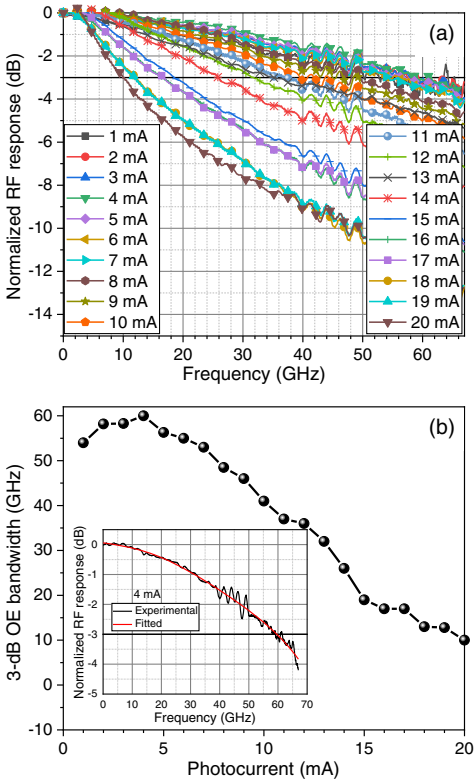

Fig. 6. (a) Normalized RF response of the Ge-on-Si PD with lateral Si_3N_4 waveguides. The bias voltage is fixed at −3 V. (b) Measured 3 dB OE bandwidths with different photocurrent levels. The inset plots the experimental and fitted results of the S21 transmission parameter under 4 mA photocurrent.

ployed WSS are about 1 nm and −5 dB. In the eye-diagram measurement process, the Ge-on-Si PD photocurrent under 1 mA is controlled by VOA. A −3 V voltage was applied to the Ge-on-Si PD with double lateral Si_3N_4 waveguides by exploiting an RF probe (cascade infinity probe GSG-125) connected to a bias tee. The output high-speed electrical data was measured with a Keysight DCA-X series wide-bandwidth sampling oscilloscope (N1000A) without using a transimpedance amplifier (TIA). Clear openings of the eye diagrams up to 70, 80, 90, and 100 Gbit/s are obtained without utilizing any offline digital signal processing (DSP) at the receiver (RX) side as shown in Fig. 7. It should be noted that the deterioration of the 100 Gbit/s eye diagram is mainly ascribed to the limited $LiNbO_3$ Mach–Zehnder modulator (MZM) with 6 dB bandwidth of 40 GHz. We believe the data reception speed of the Ge-on-Si PD with double lateral Si_3N_4 waveguides can be further improved by using a $LiNbO_3$ MZM with 6 dB bandwidth larger than 60 GHz. As shown in Fig. 8, the clear open electrical eye diagrams up to 100, 120, 140, and 150 Gbit/s PAM-4 are also attained using the proposed Ge-on-Si PD. The achieved large-signal eye diagram measurements in Figs. 7 and 8 indicate a favorable performance of the Ge-on-Si PD with double lateral Si_3N_4 waveguides under small input optical power. We believe that the proposed Ge-on-Si PD device possesses the great potential to achieve low-cost >100 Gbit/s data reception per lane for future 400/800 GbE transceivers.

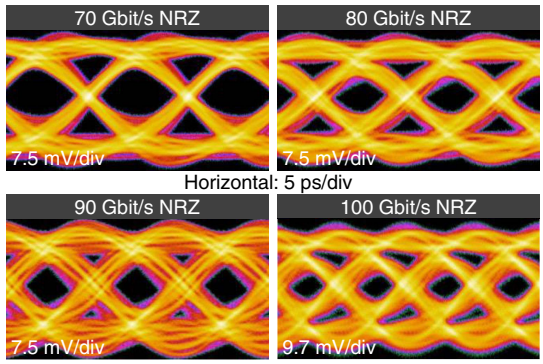

Fig. 7. Measured 70, 80, 90, and 100 Gbit/s NRZ eye diagrams under 3 V reverse-bias voltage.

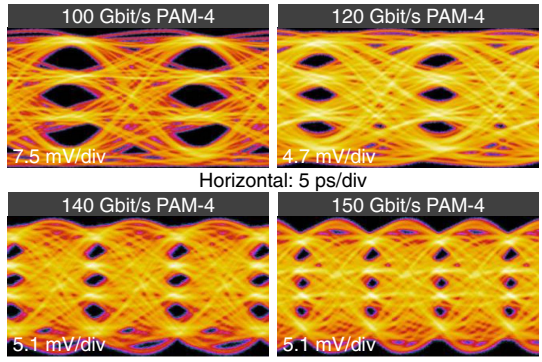

Fig. 8. Measured 100, 120, 140, and 150 Gbit/s PAM-4 eye diagrams under 3 V reverse-bias voltage.

Like the aforementioned uniform optical field distribution in Ge absorption region, it may be beneficial to improving the operation speed for high input optical power. To confirm the high-power handling performances in high-speed data transmission, the 60 Gbit/s NRZ modulated signals at different photocurrent levels are used as shown in Fig. 9. When the photocurrent increases from 5 to 15 mA, the eye diagrams are very clear. However, with the photocurrent increasing from 10 to 15 mA, there is no improvement in the eye opening or eye amplitude for the proposed Ge-on-Si PD. So the linear range of eye opening versus photocurrent can be supposed

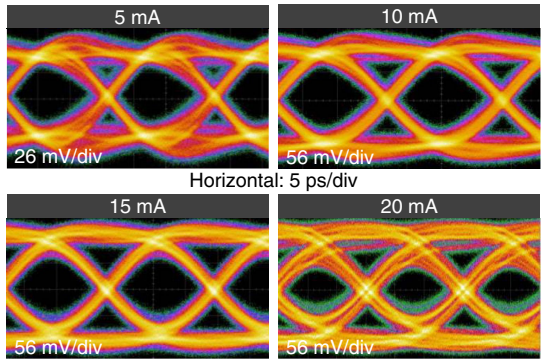

Fig. 9. Measured 60 Gbit/s NRZ eye diagrams with 5, 10, 15, and 20 mA photocurrent at the DC bias voltage of −3 V.

to be less than 10 mA. Additionally, it is interesting to see that the eye diagrams are very clear without obvious signal degradation under 10 mA and 15 mA. Even under 20 mA photocurrent, the eye diagram is still clearly open but with little electrical noise. To the best of our knowledge, this is the first work that shows clear open electrical eye diagrams of 60 Gbit/s NRZ under 20 mA photocurrent. The demonstrated results indicate that the proposed Ge-on-Si PD with double lateral Si_3N_4 waveguides also possesses the high-speed and high-power detection capability.

4. DISCUSSION

Compared to the butt-coupling scheme, the possible freely chosen parameters of an evanescent-coupling configuration based on double lateral Si_3N_4 waveguides include waveguide thickness, gap width, and waveguide shape (strip or rib or tapered waveguide and so on). One difference between the coupling configuration of the Si_3N_4 waveguide on top and on the double lateral sides of the absorber is the way to adjust the gap width between the Si_3N_4 and the absorber. For the Si_3N_4 waveguide on top of the absorber, in order to change the gap width, the thickness of the silica (SiO_2) layer has to be adjusted during the fabrication processes. Nevertheless, for the Si_3N_4 waveguide on the double lateral sides of the absorber, the variation of gap width can be realized just by designing the layout. It is very easy and accessible. Another difference is the light evanescent coupling from one side and both sides. For high input optical power, it is well known that the capability to manipulate the optical field in the absorption region to attain uniform photocarrier distribution is very beneficial to improving quantum efficiency and operation speed [34,39,42,43]. The evanescent coupling from both sides has the advantage of manipulating the optical field in the absorber. Although the lateral Si_3N_4 waveguides can be designed relatively free, in order to achieve high coupling efficiency, there are still trade-offs between Ge absorber thickness, gap width, and Si_3N_4 waveguide thickness [33].

In our proposed structure, the silicon-based 1×2 MMI splitter and the two Si to Si_3N_4 inter-layer transitions are integral parts of the proposed Ge-on-Si PD. The losses of the silicon-based 1×2 MMI splitter and Si to Si_3N_4 inter-layer transition are about 0.3 dB and 0.2 dB, respectively. The responsivity of the Ge-on-Si PD is about 0.36 A/W without correcting for the losses of these components (0.5 dB). In future designed structures, the silicon-based 1×2 MMI splitter and Si to Si_3N_4 inter-layer transitions can be replaced by a Si_3N_4-based 1×2 MMI splitter, which might further decrease the losses and improve the internal responsivity. The evanescent coupling from both sides will lead to a standing wave pattern in the absorber as shown in Fig. 2(d). This phenomenon is similar to the Ge-on-Si PD with four-directional light input [42], but its effect on optical signal reception can be nearly ignored.

5. CONCLUSION

In summary, as a proof-of-concept demonstration, we have proposed a novel light coupling scheme of waveguide-integrated Ge-on-Si PD: lateral coupling by employing double lateral Si_3N_4 waveguides. It features uniform optical field distribution in the Ge absorption region and allows for independent optimization of quantum efficiency, operation speed, and power handling. The maximum responsivity is estimated to be approximately 0.52 A/W with 25 mW input power at 1550 nm, which can be further enhanced by decreasing the gap between the Si_3N_4 waveguide and the 220 nm Si slab and increasing the gap between the Si_3N_4 waveguide and the metal copper. Based on the equivalent circuit model and extracted parameters, the Ge-on-Si PDs with double lateral Si_3N_4 waveguides have reached theoretical 3 dB OE bandwidths of up to 60.8 GHz, which is well matched to the experimentally demonstrated 60 GHz under 4 mA photocurrent at DC bias voltage −3 V. Under 1 mA photocurrent, the 70, 80, 90, and 100 Gbit/s NRZ and 100, 120, 140, and 150 Gbit/s PAM-4 clear openings of the eye diagrams are obtained without utilizing any offline DSP at the RX side. The clear open electrical eye diagrams of 60 Gbit/s NRZ under 5, 10, 15, and 20 mA photocurrent at the DC bias voltage of −3 V are also attained, which exhibits the detection capability of high-speed and high-power signal. We are currently making great efforts to improve the quantum efficiency and further explore the high-speed and high-power handling ability of Ge-on-Si PD with double lateral Si_3N_4 waveguides. Overall, the proposed lateral Si_3N_4 waveguide structure is flexibly extendable to the light coupling scheme, which shows favorable performances. It is believed that our proposed Ge-on-Si PD has the great potential to achieve low-complexity and low-cost >100 Gbit/s data reception per lane for future 400/800 GbE transceivers, which can be utilized in data centers, long-haul telecommunication, and high-performance computers. The characteristic of high-speed and wide-input-power dynamic range makes it attractive to integrated microwave photonics application, such as ultra-broadband wireless communication.

Funding. National Key Research and Development Program of China (2019YFB2205201, 2019YFB2205203); Hubei Technological Innovation Project (2019AAA054); Natural Science Foundation of Hubei Province (2019CFB216).

Disclosures. The authors declare no conflicts of interest.

REFERENCES

1. R. A. Soref, "Silicon-based optoelectronics," Proc. IEEE **81**, 1687–1706 (1993).
2. D. A. B. Miller, "Device requirements for optical interconnects to silicon chips," Proc. IEEE **97**, 1166–1185 (2009).
3. M. Asghari and A. V. Krishnamoorthy, "Energy-efficient communication," Nat. Photonics **5**, 268–270 (2011).
4. D. Thomson, A. Zilkie, J. E. Bowers, T. Komljenovic, G. T. Reed, L. Vivien, D. Marris-Morini, E. Cassan, L. Virot, J. M. Fédéli, J.-M. Hartmann, J. H. Schmid, D. X. Xu, F. Boeuf, P. O'Brien, G. Z. Mashanovich, and M. Nedeljkovic, "Roadmap on silicon photonics," J. Opt. **18**, 073003 (2016).
5. K. Yamada, T. Tsuchizawa, H. Nishi, R. Kou, T. Hiraki, K. Takeda, H. Fukuda, Y. Ishikawa, K. Wada, and T. Yamamoto, "High-performance silicon photonics technology for telecommunications applications," Sci. Technol. Adv. Mater. **15**, 024603 (2014).
6. G. Zhang, J. Y. Haw, H. Cai, F. Xu, S. M. Assad, J. F. Fitzsimons, X. Zhou, Y. Zhang, S. Yu, J. Wu, W. Ser, L. C. Kwek, and A. Q. Liu, "An

integrated silicon photonic chip platform for continuous-variable quantum key distribution," Nat. Photonics **13**, 839–842 (2019).
7. Y. Shen, N. Harris, S. Skirlo, M. Prabhu, T. Baehr-Jones, M. Hochberg, X. Sun, S. Zhao, H. Larochelle, D. Englund, and M. Soljačić, "Deep learning with coherent nanophotonic circuits," Nat. Photonics **11**, 441–446 (2017).
8. D. Marpaung, J. Yao, and J. Capmany, "Integrated microwave photonics," Nat. Photonics **13**, 80–90 (2019).
9. D. Marris-Morini, V. Vakarin, J. M. Ramirez, Q. Liu, A. Ballabio, J. Frigerio, M. Montesinos, C. Alonso-Ramos, X. Le Roux, S. Serna, D. Benedikovic, D. Chrastina, L. Vivien, and G. Isella, "Germanium based integrated photonics from near- to mid-infrared applications," Nanophotonics **7**, 1781–1793 (2018).
10. J. Michel, J. Liu, and L. C. Kimerling, "High-performance Ge-on-Si photodetectors," Nat. Photonics **4**, 527–534 (2010).
11. Y. Ishikawa, K. Wada, D. D. Cannan, J. Liu, D. L. Hsin-Chiao, and L. C. Kimerling, "Strain-induced band gap shrinkage in Ge grown on Si substrate," Appl. Phys. Lett. **82**, 2044–2046 (2003).
12. J. F. Liu, J. Michel, W. Giziewicz, D. Pan, K. Wada, D. Cannon, L. C. Kimerling, J. Chen, F. O. Ilday, F. X. Kartner, and J. Yasaitis, "High-performance, tensile strained Ge p-i-n photodetectors on a Si platform," Appl. Phys. Lett. **87**, 103501 (2005).
13. R. Anthony, D. E. Hagan, D. Genuth-Okon, L. M. Maestro, I. F. Crowe, M. P. Halsall, and A. P. Knights, "Extended wavelength responsivity of a germanium photodetector integrated with a silicon waveguide exploiting the indirect transition," IEEE J. Sel. Top. Quantum Electron. **26**, 3800107 (2020).
14. H. Chen, M. Galili, P. Verheyen, P. De Heyn, G. Lepage, J. De Coster, S. Balakrishnan, P. Absil, L. Oxenlowe, J. Van Campenhout, and G. Roelken, "100-Gbps RZ data reception in 67-GHz Si-contacted germanium waveguide p-i-n photodetectors," J. Lightwave Technol. **35**, 722–726 (2017).
15. M. Rouviere, M. Halbwax, J.-L. Cercus, E. Cassan, L. Vivien, D. Pascal, M. Heitzmann, J.-M. Hartmann, and S. Laval, "Integration of germanium waveguide photodetectors for intrachip optical interconnects," Opt. Eng. **44**, 75402–75406 (2005).
16. D. Dai, M. Piels, and J. E. Bowers, "Monolithic germanium/silicon photodetectors with decoupled structures: resonant APDs and UTC photodiodes," IEEE J. Sel. Top. Quantum Electron. **20**, 3802214 (2014).
17. L. Colace, G. Masini, F. Galluzzi, G. Assanto, G. Capellini, L. Di Gaspare, E. Palange, and F. Evangelisti, "Metal-semiconductor-metal near-infrared light detector based on epitaxial Ge/Si," Appl. Phys. Lett. **72**, 3175–3177 (1998).
18. H. C. Luan, D. R. Lim, K. K. Lee, K. M. Chen, and L. C. Kimerling, "High-quality Ge epilayers on Si with low threading-dislocation densities," Appl. Phys. Lett. **75**, 2909–2911 (1999).
19. M. Halbwax, D. Bouchier, V. Yam, D. Debarre, L. H. Nguyen, Y. Zheng, P. Rosner, M. Benamara, H. P. Strunk, and C. Clerc, "Kinetics of Ge growth at low temperature on Si (001) by ultrahigh vacuum chemical vapor deposition," J. Appl. Phys. **97**, 064907 (2005).
20. J. Liu, R. Camacho-Aguilera, J. T. Bessette, X. Sun, X. Wang, Y. Cai, L. C. Kimerling, and J. Michel, "Ge-on-Si optoelectronics," Thin Solid Films **520**, 3354–3360 (2012).
21. L. Chen, P. Dong, and M. Lipson, "High performance germanium photodetectors integrated on submicron silicon waveguides by low temperature wafer bonding," Opt. Express **16**, 11513–11518 (2008).
22. Z. Huang, J. Oh, and J. C. Campbell, "Back-side-illuminated high-speed Ge photodetector fabricated on Si substrate using thin SiGe buffer layers," Appl. Phys. Lett. **85**, 3286–3288 (2004).
23. D. Ahn, C. Hong, J. Liu, W. Giziewicz, M. Beals, L. C. Kimerling, and J. Michel, "High performance, waveguide integrated Ge photodetectors," Opt. Express **15**, 3916–3921 (2007).
24. X. Li, L. Peng, Z. Liu, X. Liu, J. Zheng, Y. Zuo, C. Xue, and B. Cheng, "High-power back-to-back dual-absorption germanium photodetector," Opt. Lett. **45**, 1358–1361 (2020).
25. H. Chen, P. Verheyen, P. De Heyn, G. Lepage, J. De Coster, P. Absil, G. Roelkens, and J. Van Campenhout, "High-responsivity low-voltage 28-Gb/s Ge p-i-n photodetector with silicon contacts," J. Lightwave Technol. **33**, 820–824 (2015).
26. H. Chen, P. Verheyen, P. De Heyn, G. Lepage, J. De Coster, S. Balakrishnan, P. Absil, W. Yao, L. Shen, G. Roelkens, and J. Van Campenhou, "–1 V bias 67 GHz bandwidth Si-contacted germanium waveguide p-i-n photodetector for optical links at 56 Gbps and beyond," Opt. Express **24**, 4622–4631 (2016).
27. Z. Liu, F. Yang, W. Wu, H. Cong, J. Zheng, C. Li, C. Xue, B. Cheng, and Q. Wang, "48 GHz high-performance Ge-on-SOI photodetector with zero-bias 40 Gbps grown by selective epitaxial growth," J. Lightwave Technol. **35**, 5306–5310 (2017).
28. D. Benedikovic, L. Virot, G. Aubin, F. Amar, B. Szelag, B. Karakus, J. M. Hartmann, C. Alonso-Ramos, X. L. Roux, P. Crozat, E. Cassan, D. Marris-Morini, C. Baudot, F. Boeuf, J. M. Fédéli, C. Kopp, and L. Vivien, "25 Gbps low-voltage hetero-structured silicon-germanium waveguide pin photodetectors for monolithic on-chip nanophotonic architectures," Photon. Res. **7**, 437–444 (2019).
29. D. Benedikovic, L. Virot, G. Aubin, J. M. Hartmann, F. Amar, B. Szelag, X. L. Roux, C. Alonso-Ramos, P. Crozat, É. Cassan, D. Marris-Morini, C. Baudot, F. Boeuf, J. M. Fédéli, C. Kopp, and L. Vivien, "Comprehensive study on chip-integrated germanium PIN photodetectors for energy-efficient silicon interconnects," IEEE J. Sel. Top. Quantum Electron. **56**, 8400409 (2020).
30. L. Vivien, M. Rouvière, J. M. Fédéli, D. Marris-Morini, J. F. Damlencourt, J. Mangeney, P. Crozat, L. E. Melhaoui, E. Cassan, X. L. Roux, D. Pascal, and S. Laval, "High speed and high responsivity germanium photodetector integrated in a silicon-on-insulator microwaveguide," Opt. Express **15**, 9843–9848 (2007).
31. C. T. DeRose, D. C. Trotter, W. A. Zortman, A. L. Starbuck, M. Fisher, M. R. Watts, and P. S. Davids, "Ultra compact 45 GHz CMOS compatible germanium waveguide photodiode with low dark current," Opt. Express **19**, 24897–24904 (2011).
32. J. Cui and Z. Zhou, "High-performance Ge-on-Si photodetector with optimized DBR location," Opt. Lett. **42**, 5141–5144 (2017).
33. D. Ahn, L. C. Kimerling, and J. Michel, "Efficient evanescent wave coupling conditions for waveguide-integrated thin-film Si/Ge photodetectors on silicon-on-insulator/germanium-on-insulator substrates," J. Appl. Phys. **110**, 083115 (2011).
34. M. J. Byrd, E. Timurdogan, Z. Su, C. V. Poulton, and M. R. Watts, "Mode-evolution-based coupler for high saturation power Ge-on-Si photodetectors," Opt. Lett. **42**, 851–854 (2017).
35. C. H. Henry, R. F. Kazarinov, H. J. Lee, K. J. Orlowsky, and L. E. Katz, "Low loss Si_3N_4-SiO_2 optical waveguides on Si," Appl. Opt. **26**, 2621–2624 (1987).
36. P. Muñoz, G. Micó, L. A. Bru, D. Pastor, D. Pérez, J. D. Doménech, J. Fernández, R. Baños, B. Gargallo, R. Alemany, A. M. Sánchez, J. M. Cirera, R. Mas, and C. Domínguez, "Silicon nitride photonic integration platforms for visible, near-infrared and mid-infrared applications," Sensors **17**, 2088 (2017).
37. C. G. H. Roeloffzen, M. Hoekman, E. J. Klein, L. S. Wevers, R. B. Timens, D. Marchenko, D. Geskus, R. Dekker, A. Alippi, R. Grootjans, A. V. Rees, R. M. Oldenbeuving, J. P. Epping, R. G. Heideman, K. Worhoff, A. Leinse, D. Geuzebroek, E. Schreuder, P. W. L. van Dijk, I. Visscher, C. Taddei, Y. Fan, C. Taballione, Y. Liu, D. Marpaung, L. Zhuang, M. Benelajla, and K. J. Boller, "Low-loss Si_3N_4 TriPleX optical waveguides: technology and applications overview," IEEE J. Sel. Top. Quantum Electron. **24**, 4400321 (2018).
38. D. J. Blumenthal, R. Heideman, D. Geuzebroek, A. Leinse, and C. Roeloffzen, "Silicon nitride in silicon photonics," Proc. IEEE **106**, 2209–2231 (2018).
39. K. S. Giboney, M. J. W. Rodwell, and J. E. Bowers, "Travelling-wave photodetector design and measurements," IEEE J. Sel. Top. Quantum Electron. **2**, 622–629 (1996).
40. A. Beling, X. Xie, and J. C. Campbell, "High-power, high-linearity photodiodes," Optica **3**, 328–338 (2016).
41. M. Oehme, J. Werner, E. Kasper, M. Jutzi, and M. Berroth, "High bandwidth Ge p-i-n photodetector integrated on Si," Appl. Phys. Lett. **89**, 071117 (2006).
42. X. Hu, D. Wu, H. Zhang, W. Li, D. Chen, L. Wang, X. Xiao, and S. Yu, "High-speed lateral PIN germanium photodetector with 4-directional light input," Opt. Express **28**, 38343–38354 (2020).
43. Y. Zuo, Y. Yu, Y. Zhang, D. Zhou, and X. L. Zhang, "Integrated high-power germanium photodetectors assisted by light field manipulation," Opt. Lett. **44**, 3338–3341 (2019).